

Photoexcited ZnO nanoparticles with controlled defects as a highly sensitive oxygen sensor

Taku Goto¹, Yoshiki Shimizu², Hidehiro Yasuda^{3,4}, and Tsuyohito Ito*¹

¹Center for Atomic and Molecular Technologies, Graduate School of Engineering,
Osaka University, Osaka 565-0871, Japan

²Nanomaterials Research Institute, National Institute of Advanced Industrial Science and
Technology (AIST), Tsukuba, Ibaraki 305-8565, Japan

³Division of Materials and Manufacturing Science, Graduate School of Engineering,
Osaka University, Osaka 565-0871, Japan

⁴Research Center for Ultra-High Voltage Electron Microscopy,
Osaka University, Osaka 565-0871, Japan

*E-mail: tsuyohito@ppl.eng.osaka-u.ac.jp

ABSTRACT

Conductance of photoexcited ZnO nanoparticles with various defects has been investigated in oxygen. ZnO nanoparticles, which show strong photoluminescence peaks originating from interstitial zinc atom (Zn_i) and singly charged oxygen vacancy (V_O^+), show oxygen-pressure-dependent conductance changes caused by photoexcitation. Herein, a model is proposed to simulate the conductance changes.

Improving the sensitivity, response time, and lifetime of semiconductor oxygen sensors, and widening their applicability are expected to influence various fields such as biological science, industrial processing, medical treatment, and agriculture. Most semiconductor oxygen sensors detect oxygen attachments on the surface, principally using chemical means. Such sensors are applicable for various gases such as CO, ethanol, H₂, and H₂O, which remove oxygen from the surface¹⁻³. Among various detection mechanisms, ultraviolet (UV) light assisted nanostructure (NS) oxygen sensors have attracted much attention because they provide benefits not only of high sensitivity^{4,5}, but also of low working temperature^{4,5}. In fact, ZnO is studied extensively for use as a UV-assisted NS oxygen sensor. Room-temperature operation of UV-assisted ZnO NS oxygen sensors has been reported. Furthermore, sensitivities of various ZnO nanoparticles have been reported according to their size and production method^{4,6}.

Actually, ZnO NS conductance is well known to respond to UV light excitation and to oxygen pressure^{5,7}. Nevertheless, those mechanisms must be elucidated further to realize highly sensitive oxygen sensors and photodetectors. For example, although a temporal change of conductance for the excited ZnO NS can be well simulated⁸, that with modification of oxygen pressure has not been achieved yet. This letter presents a simulation of temporal changes as functions of oxygen pressure and UV power. The simulations provide useful models for photodetectors and oxygen sensors. Furthermore, results suggest that an oxygen sensor can be operated using the initial temporal change instead of equilibrium conductivity (requiring >0.3 s in our case), the response time can be shortened considerably. The model presented in this report includes the assumption that the electron conduction channel is reduced by a depletion layer caused by chemisorbed oxygen at the oxygen chemisorption site³. Results of this study suggest that the effective ZnO NSs sensor requires not only singly charged oxygen vacancy (V_{O}^+), but also interstitial

zinc atoms (Zn_i). We believe that the energy of Zn_i is close to the conduction band because the existence of shallow defects has been reported for sensitive sensors⁹.

For our study, we applied nanoparticles (NPs) as NSs. The ZnO NPs were prepared using laser ablation in water–ethanol mixtures. The liquid pressure and the concentrations are modified to generate various NPs. Details obtained from synthesis and photoluminescence (PL) spectroscopy of the generated NPs have been presented in our previous report¹⁰. Table 1 presents the relative PL signal ratios for several peaks for several processing conditions. The near band edge peak reported earlier is now assigned to a zinc vacancy defect¹¹.

To produce the test devices, the NPs are cast on platinum interdigitated electrodes (10 μm width electrodes separated by 10 μm space) with area of approximately 35 mm^2 and dried at the moderate temperature of 40 $^\circ\text{C}$.

Temporal change of the conductivity of the ZnO electrodes after photoexcitation was investigated in pure oxygen with various pressures. For photoexcitation, a He-Cd laser at 325 nm is irradiated for the NPs sitting on the electrodes. The power density of UV light was 3.1 mW/mm^2 . The irradiated area was approximately 2.5 mm^2 . The current growth after the photoexcitation was recorded as the voltage drop at the shunt of 10 $\text{k}\Omega$ with constant applied voltage of 1.75 V. The voltage across the ZnO electrodes varied from 0.6 V to 1.75 V during measurements. The resistance curve is generated from the current and voltage curves calculated using Ohm's law. We confirmed that the resistance is independent of the voltage in the tested conditions used for this study.

Although we tested several samples for each synthesis condition, no response was observed with those prepared in pure and 50% water, irrespective of the pressure during synthesis. Oscillographs show only flat lines. They are therefore omitted here. However, the samples produced with ZnO NPs synthesized in 99.5 vol% ethanol show clear response to the photoexcitation. The

response varies with the oxygen pressure. Examples are presented in Fig. 1 for NPs generated in high-pressure (8 MPa) ethanol and in Fig. 2 for those generated in atmospheric pressure (0.1 MPa).

All long-term oscillograms shown in Figs. 1(a) and 2(a) portray a common feature: increase from nearly zero conductivity and then a plateau. The initial rise and the value at the plateau depend on the oxygen pressure. Higher pressure shows lower values (given the same electrodes). The initial tilt (shown in the Figs. 1(b) and 2(b)) is depicted in Fig. 3 as a function of oxygen pressure, with theoretical fittings described below. The initial rise decreases continuously with the oxygen-pressure increase. It is particularly interesting that the slopes differ among liquid pressures during laser ablation.

Comparing the contrasting conductance changes with PL peak intensities shown in Table 1, it can be inferred that shallow defects reported by Sharma et al.⁹ are Zn_i, with energy level that is reportedly 0.09–0.3 eV less than that of the conduction band¹². Furthermore, V_O⁺ is expected to play an important role, which we strongly believe based on results of the following analysis, acts as the chemisorption sites of oxygen. This role is probably similar to that of the oxygen vacancy in TiO₂, working as oxygen chemisorption site¹³.

Experimental responses of the conductance are analyzed further using a model that incorporates (i) conduction-band electron (e⁻) and hole (h⁺) generation by photoexcitation (hν_{ex})¹⁴; (ii) oxygen (O₂) chemisorption at the site (site_{O₂}) and forming ionized oxygen (O₂⁻) and vice versa; (iii) recombination of the adsorbed electron (in O₂⁻) and the hole (h⁺) with oxygen detachment (iv)¹⁵, and (v) recombination of the electrons (e_C⁻) and holes (h_C⁺) at a recombination center (C) with photo-emission (hν_{em}). By the latest assumption (v), the recombination center density is assumed to be constant because the density is generally very high^{9,14}. Consequently, the electron and hole lifetimes are mutually independent. The processes described above are presented in Table 2 as six

reactions. The existence of these processes is supported by previous reports^{3,9,14,15}. Assumptions we have made to fit the temporal change of the conductance are that (vi) the nominal area of the electron conduction channel is reduced by the depletion layer, and that the area reduction rate is proportional to the chemisorbed oxygen density. These assumptions are supported qualitatively by the fact that the conductance of a ZnO nanowire decreases concomitantly with increasing ambient oxygen pressure¹⁷. Furthermore, the current is assumed to be carried dominantly by conduction-band electrons. The hole current is neglected in our analysis presented here. Consequently, conductance (an inverse of the resistance R (Ω)) can be described as

$$\frac{1}{R} = \frac{1}{C_0 - \left(\frac{C_1 L}{A_0 - K [O_2^-]} \right) [e^-]} \cdots (1),$$

where $[]$ denotes the density (m^{-3}), C_0 signifies the base resistance for unit electron density including contact resistance ($\Omega \cdot m^{-3}$), C_1 denotes the resistance of natural ZnO for a unit area and electron density per unit length ($\Omega \cdot m^{-2}$), A_0 represents the maximum area of the electron conduction channel of ZnO NPs (m^2), K signifies the coefficient for the area reduction by an adsorbed O_2 molecule (m^5), and L is the effective length of the conduction channel (m).

From the six reactions in Table 2, the rate equations for variable densities of e^- , O_2^- , and h^+ are the following three.

$$\frac{d[e^-]}{dt} = -P_{O_2} r_1 \left(1 - \frac{[O_2^-]}{[site_{O_2}]} \right) + B_{kl} - \frac{[e^-]}{\tau_e} + r_2 [O_2^-] \cdots (2)$$

$$\frac{d[O_2^-]}{dt} = P_{O_2} r_1 \left(1 - \frac{[O_2^-]}{[site_{O_2}]} \right) - r_2 [O_2^-] - k_1 [h^+] [O_2^-] \cdots (3)$$

$$\frac{d[h^+]}{dt} = -k_1 [h^+] [O_2^-] + B_{kl} - \frac{[h^+]}{\tau_h} \cdots (4)$$

Therein, P_{O_2} represents the oxygen pressure (Pa). r_1 is the reaction constant of the oxygen chemisorption on the oxygen chemisorption site ($\text{kg}^{-1}\text{m}^{-2}\text{s}$). r_2 is the reaction constant for the oxygen desorption from the chemisorption site (s^{-1}). B_{kl} is the density of charge carriers generated per second under UV illumination ($\text{m}^{-3}\text{s}^{-1}$). τ_e and τ_h are the electron and hole lifetime (s). Also, k_1 is the reaction constant for the recombination of the adsorbed electron (in O_2) and the hole (m^3s^{-1}).

While maintaining equilibrium $[\text{O}_2]$ density in cases without photoexcitation and assuming a linear rise of $[e^-]$, and therefore a negligibly small initial density and no decay process, one can obtain the initial tilt of $1/R$ (conductance) by inserting $[e^-]$ and $[\text{O}_2]$ into eq. (1) as shown below.

$$\frac{d\left(\frac{1}{R}\right)}{dt} = \frac{1}{C_0 \left\{ A_0 - K \left(\frac{C_1 L}{r_1 + \frac{r_2 [\text{site}_{\text{O}_2}]}{P_{\text{O}_2}}} \right) \right\}} B_{\text{kl}} \dots (5)$$

Indeed, the dependence of the initial tilt on the oxygen pressure is apparent in Fig. 1(b) and Fig. 2(b). Furthermore, we experimentally confirmed a linear relation between UV-light intensity and the initial tilt (results not shown), as suggested by eq. (5). Revisiting Fig. 3, it shows theoretical fitting by eq. (5). In this fitting, a product of r_2 and $[\text{site}_{\text{O}_2}]$ for ZnO NPs synthesized at high pressure is more than 20 times greater than those synthesized in atmospheric pressure. The difference shows that more oxygen chemisorption sites on ZnO NPs produced at high pressure if one assumes a similar r_2 (reaction constant of the oxygen desorption from the chemisorption site).

We assumed that this difference is attributable to the different particle sizes between the pressures during syntheses. Our previous work suggests that the particle size decreases with ambient

pressure increase¹⁷. With a decrease of ZnO NPs size, the surface oxygen chemisorption sites increase. Consequently, it is reasonable to infer that the density of the O₂ chemisorption sites, which we believe are surface V_O⁺ defects, is higher on the ZnO NPs produced at higher pressure.

Finally, Fig. 4 presents a simulation of the temporal change of the conductance of ZnO NPs electrodes after UV-light irradiation. The examples presented in Fig. 4 portray results obtained for ZnO NPs synthesized at atmospheric pressure. These theoretical curves apply constants from eq. (5) fitted to the initial tilts, then other parameters in eqs. (2)–(4) are modified to provide best fit to the curves portrayed in Fig. 4. Reasonably good agreement was found, indicating that the model and assumptions are acceptable to produce the temporary change of conductance. The fitting parameters applied here were, for example, B_{kl} of $5.1 \times 10^{29} \text{ (m}^{-3}\text{s}^{-1}\text{)}$ under the UV intensity of 3.1 mW/mm^2 , resulting in the ratio of B_{kl} to the UV intensity to be $1.7 \times 10^{26} \text{ m}^{-1}\text{s}^{-1}\text{W}^{-1}$, $[\text{site}_{\text{O}_2}]$ of $3.9 \times 10^{22} \text{ (m}^{-3}\text{)}$, and k_r of $1.0 \times 10^{-20} \text{ (m}^{-3}\text{s}^{-1}\text{)}$. The reported value for the B_{kl} of ZnO synthesized by RF diode sputtering is $6.3 \times 10^{26} \text{ (m}^{-3}\text{s}^{-1}\text{)}$ with UV intensity of $20 \text{ }\mu\text{W/cm}^2$, and therefore equal to $3.2 \times 10^{27} \text{ m}^{-1}\text{s}^{-1}\text{W}^{-1}$,⁸ which is of similar order to ours. Furthermore, the oxygen chemisorption site shows a similar value to the reported V_O⁺ density¹⁸.

In summary, the conductance of the photoexcited ZnO NPs which show different PL spectra was measured in oxygen. Only ZnO NPs that show strong V_O⁺ and Zn_i PL peaks respond to the photoexcitation depending on the oxygen pressure. Therefore, we believe that Zn_i and V_O⁺ play important roles. The earlier are expected to be the shallow defects, as Sharma et al. reported. The latter are expected to act as an oxygen chemisorption site. Moreover, the reaction model, which can quantitatively reproduce conduction changes at various oxygen pressures, is proposed. Curve fitting to experimental data revealed that high pressure during particle synthesis can generate more surface V_O⁺ defects.



This manuscript was accepted by Appl. Phys. Lett. Click [here](#) to see the version of record.

We thank Mr. Sakata for his technical support. Osaka University Microstructural Characterization Platform supported part of this work as a “Nanotechnology Platform” program of the Ministry of Education, Culture, Sports, Science and Technology (MEXT), Japan.

ACCEPTED MANUSCRIPT

REFERENCES

- [1] S. Prabakaran and J. B. B. Rayappan, *ScienceJet* **4**, 1 (2015).
- [2] S. Choopun, N. Hongsoth, P. Mangkorntong, and N. Mangkorntong, *Physica E*. **39**, 53 (2007).
- [3] O. Lupan, V. V. Ursaki, G. Chai, L. Chow, G. A. Emelchenko, I. M. Tiginyanu, A. N. Gruzintev, and A. N. Redkin, *Sensor. Actuat. B – Chem.* **144**, 56 (2010).
- [4] H. K. Yadav, K. Sreenivas, and V. Gupta, *J. Appl. Phys.* **107**, 044507 (2010).
- [5] J. K. Park, D. E. Song, and S. S. Kim, *Nanotechnology* **19**, 105503 (2008).
- [6] J. Eriksson, V. Khranovskyy, F. Söderlind, P.-O. Käll, R. Yakimova, and A. L. Spetz, *Sensor Actuat. B – Chem.* **137**, 94 (2009).
- [7] L. Oleg, L. Chow, and G. Chai, *Sensor. Actuat. B – Chem.* **141**, 511 (2009).
- [8] H. K. Yadav, and V. Gupta, *J. Appl. Phys.* **111**, 102809 (2012).
- [9] P. Sharma, K. Sreenivas, and K. V. Rao, *J. Appl. Phys.* **93**, 3963 (2003).
- [10] T. Goto, M. Honda, S.A. Kulinich, Y. Shimizu, and T. Ito, *Jpn. J. Appl. Phys.* **54**, 070305 (2015).
- [11] S.-H. Jeong, B.-S. Kim, and B.-T. Lee, *Appl. Phys. Lett.* **82**, 2625 (2003).
- [12] A. A. Sokol, S. A. French, S. T. Bromley, C. R. A. Catlow, H. J. J. van Dam, and P. Sherwood, *Faraday Discuss.* **134**, 267 (2007).
- [13] G. Lu, A. Linsebigler, and J. T. Yates Jr., *J. Chem. Phys.* **102**, 4657 (1995).
- [14] S. M. Ryvkin, Photoelectric Effect in Semiconductors (Consultants Bureau), New York, 1964.

- [15] Y. Jin, J. Wang, B. Sun, J. C. Blakesley, and N. C. Greenham, *Nano Lett.* **8**, 1649 (2008).
- [16] Q. H. Li, X. Y. Liang, Q. Wan, and T. H. Wang, *Appl. Phys. Lett.* **85**, 6389 (2004).
- [17] S. A. Kulinich, T. Kondo, Y. Shimizu, and T. Ito, *J. Appl. Phys.* **113**, 033509 (2013).
- [18] K. Vanheusden, C. H. Seager, W. L. Warren, D. R. Tallant, J. Caruso, M. J. Hampden-Smith, and T. T. Kodas, *J. Lumin.* **75**, 11 (1997).

ACCEPTED MANUSCRIPT

Table 1. Relative ratios (%) of PL peak area for several processing conditions¹⁰

Medium type	Water		50 vol.% water – 50 vol.% ethanol		Ethanol (99.5 vol.%)	
	1 atm	13 MPa	1 atm	13 MPa	1 atm	8 MPa
Near band edge (zinc vacancy (V_{Zn}))	1.9	1.3	5.6	1.2	2.4	2.3
Interstitial zinc atom to zinc vacancy (Zn_i-V_{Zn})	2.9	1.3	5.6	5.8×10^{-3}	20	19
Plus charged oxygen vacancy (V_O^+)	5.2	3.7	22	5.9	26	27
Interstitial oxygen atom (O_i)	69	73	41	48	28	28
Double charged oxygen vacancy (V_O^{++})	20	20	26	41	24	25

Table 2. Reactions considered for a photo-assisted oxygen response model

$h\nu_{\text{ex}} \rightarrow e^{-} + h^{+}$
$O_{2(\text{gas})} + \text{site}_{O_2} + e^{-} \rightleftharpoons O_2^{-}$
$O_2^{-} + h^{+} \rightarrow O_{2(\text{gas})} \uparrow + \text{site}_{O_2}$
$e^{-} + C \rightarrow e_c^{-} + C$
$h^{+} + C \rightarrow h_c^{+} + C$
$e_c^{-} + h_c^{+} \rightarrow h\nu_{\text{em}}$

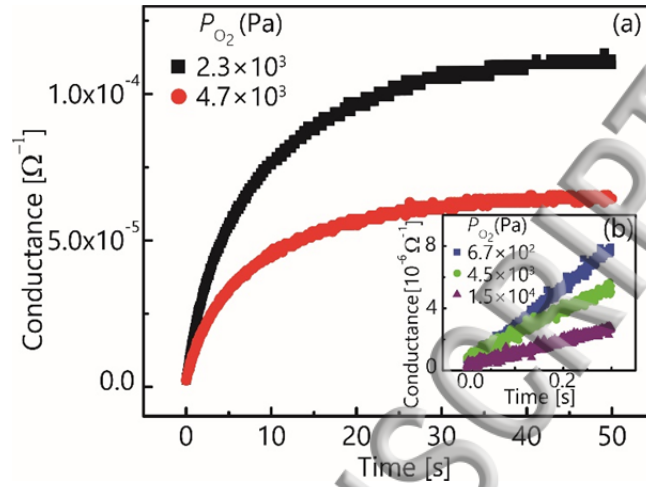


FIG. 1. Conductance–time curves of ZnO NPs synthesized in high-pressure (8 MPa) ethanol: (a) long-term curves for two surrounding oxygen pressures and (b) short-term curves for three oxygen pressures after UV irradiation at 0 s.

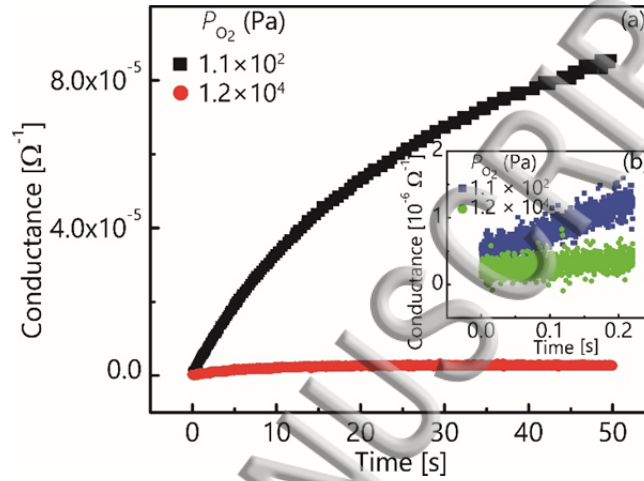


FIG. 2. Conductance–time curves of ZnO NPs synthesized in atmospheric-pressure ethanol: (a) long-term and (b) short-term curves for two surrounding oxygen pressures after UV irradiation at 0 s.

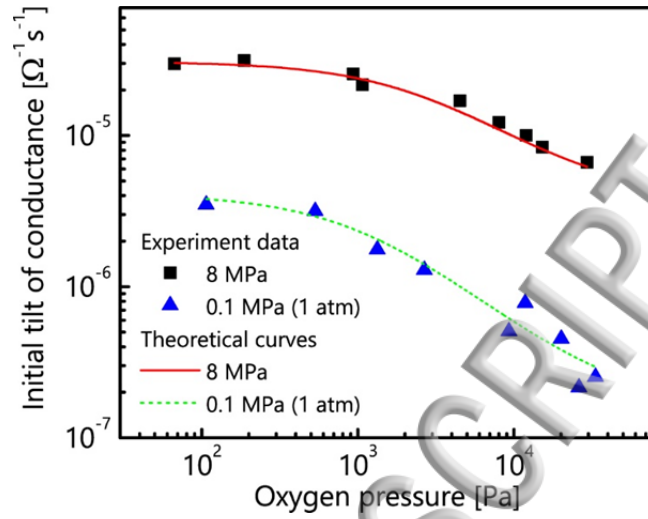


FIG. 3. Initial tilts of conductance as functions of surrounding oxygen pressure. Pressures for synthesis are 8 MPa (■, black squares) and 0.1 MPa (▲, blue triangles). Lines are simulated curves.

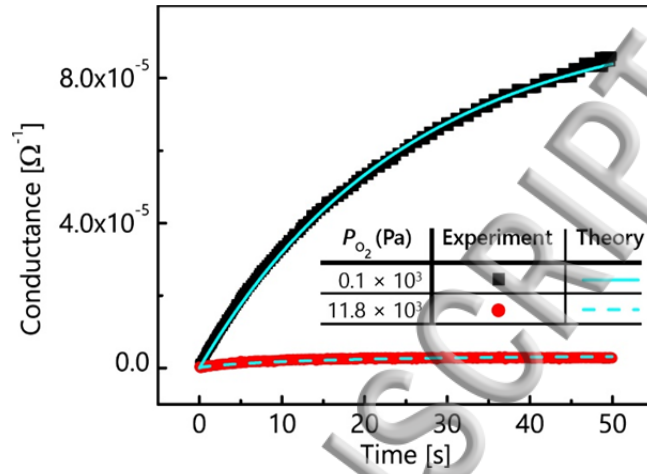


FIG. 4. Conductance–time curves (symbols) of ZnO NPs synthesized in atmospheric-pressure ethanol for two surrounding oxygen pressures as well as the fitted theoretical curves (lines).

